Austenite Stability Effects on Tensile Behavior of Manganese-Enriched-Austenite Transformation-Induced Plasticity Steel

P.J. GIBBS, E. DE MOOR, M.J. MERWIN, B. CLAUSEN, J.G. SPEER, and D.K. MATLOCK

Manganese enrichment of austenite during prolonged intercritical annealing was used to produce a family of transformation-induced plasticity (TRIP) steels with varying retained austenite contents. Cold-rolled 0.1C-7.1Mn steel was annealed at incremental temperatures between 848 K and 948 K (575 °C and 675 °C) for 1 week to enrich austenite in manganese. The resulting microstructures are comprised of varying fractions of intercritical ferrite, martensite, and retained austenite. Tensile behavior is dependent on annealing temperature and ranged from a low strain-hardening "flat" curve to high strength and ductility conditions that display positive strain hardening over a range of strain levels. The mechanical stability of austenite was measured using *in-situ* neutron diffraction and was shown to depend significantly on annealing temperature. Variations in austenite stability between annealing conditions help explain the observed strain hardening behaviors.

DOI: 10.1007/s11661-011-0687-y

I. INTRODUCTION

RESEARCH on new advanced high strength steels (AHSS) has led to the development of steel grades with improved property ranges as required by new automotive designs optimized for fuel efficiency and safety.[1,2] Current "first generation" AHSS grades are based predominantly on ferritic microstructures with the addition of low-temperature transformation products (bainite, martensite, and carbon-enriched austenite) to increase strength; these steel grades include dual-phase (DP), transformation-induced plasticity (TRIP), complex-phase, and martensitic steels. While the properties displayed by these steels are impressive, there is a desire to develop steels with improved formability at a given strength level.[1] Austenitic steels, including stainless steels and recently developed twinning-induced plasticity steels (TWIP), exhibit excellent combinations of strength and ductility and constitute a group of steels referred to as the "second generation" AHSS. However, stabilization of the fully austenitic structure requires high alloy levels, and thus, the steels are expensive and have received limited use in the commercial automotive industry.

An opportunity exists to develop a new family of steels with properties between the first and second generation steels addressing the limitations of each. These "third generation" AHSS grades are of great interest and there is considerable research effort being focused on their development.[2] In comparison to the first generation steels, it is anticipated that these steels will have increased amounts of retained austenite with controlled stability against strain-induced transformation to martensite.[3,4]

One approach to develop microstructures of interest uses lean alloys (5 to 8 wt pct Mn) and intercritical annealing in the ferrite-austenite region to enrich austenite in Mn, thus stabilizing it to room temperature. Significant austenite fractions (20 to 40 pct) have been obtained in this way depending on processing and Mn content.[9–18]

A methodology for identifying heat treatment conditions for optimal Mn enrichment has been developed based on an equilibrium thermodynamic analysis.[5,6] Predictions of austenite amount and composition as a function of annealing temperature were made using THERMO-CALC* software with the TCFE2 database for a 0.1-C 7.1-Mn 0.1-C steel, and the predicted austenite C, Mn, and Si contents are shown in Figure 1.[7,8] With a decrease in annealing temperature from 913 K to 723 K (640 °C to 450 °C), the equilibrium Mn content in austenite increases from 10 to 25 wt pct. Additionally, the predicted C content in austenite exhibits a peak at around 873 K (600 °C), while the predicted Si content remains essentially constant. A model was

*THERMO-CALC is a trademark of Thermo-Calc, Stockholm.

P.J. GIBBS, Graduate Student, E. DE MOOR, Research Faculty, and J.G. SPEER and D.K. MATLOCK, Professors, are with the Advanced Steel Processing and Products Research Center, Colorado School of Mines, Golden, CO 80401. Contact e-mail: pgibbs@mines.edu M.J. MERWIN, Research Consultant, is with the United States Steel Corporation Research and Technology Center, Munhall, PA 15120. B. CLAUSEN, SMARTS Instrument Scientist, is with the Los Alamos Neutron Science Center, Los Alamos National Laboratory, Los Alamos, NM 87545.

Manuscript submitted January 13, 2011.
Article published online April 27, 2011

used to predict the amount of austenite stabilized to room temperature through enrichment of austenite with Mn and C during intercritical annealing.[6] The resulting predicted fraction of stabilized austenite as a function of annealing temperature is shown in Figure 2. A peak in the predicted amount of retained austenite is observed at approximately 873 K (600 °C), where, as shown in Figure 1, the C content of the austenite is maximized and significant Mn enrichment is predicted. Also included in Figure 2 are experimentally measured austenite contents, as discussed subsequently.

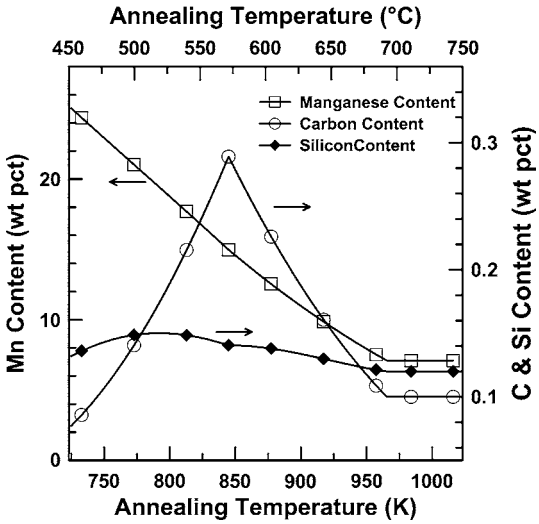

Fig. 1—Predicted equilibrium austenite composition as a function of annealing temperature for 7.1-Mn 0.1-C 0.15-Si steel. Calculations performed using THERMO-CALC and the TCFE2 database.[7,8]

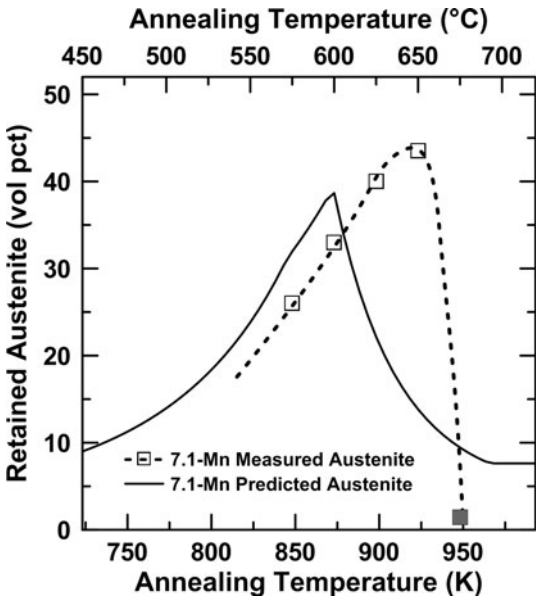

Fig. 2—Austenite fraction as a function of annealing temperature for 0.1-C7.1-Mn0.12-Si steel, as predicted by the model developed by De Moor and as measured by neutron diffraction (open symbol) and XRD (shaded symbol) after 1 week annealing.[6]

A wide range of tensile behaviors and properties are observed in Mn-TRIP steels depending on processing conditions and alloy composition.[9–18] The observed tensile behavior is highly dependent on processing conditions and annealing temperature. Steels with radically different flow behavior, including discontinuous yielding, positive strain hardening, and serrated flow behavior at high strains have been observed.[9,11–18] Differences in mechanical behavior may be explained in part by the dependence of the mechanical stability of austenite on variations in processing history.

The present work investigates austenite stability in a 7.1-Mn steel intercritically annealed to enrich austenite in Mn. Measurements of austenite fraction with strain were made and correlated to the observed tensile behavior. Additionally, two models for strain-induced austenite decomposition[19–23] were fit to the measured austenite fraction data to develop an understanding of the transformation behavior.

II. EXPERIMENTAL METHODS

A 7.1-Mn steel with the composition shown in Table I was used for the present study. This steel, used in previous batch annealing studies by Merwin,[11–13] was vacuum cast and hot rolled to 4 mm and air cooled. A fully martensitic hot-rolled structure was obtained. The sheet was then surface ground and cold rolled 50 pct to a final thickness of 1.5 mm. Using the methodology discussed with Figure 2, heat treatments between 848 K and 948 K (575 °C and 675 °C) in 25 deg increments were identified to investigate a range of predicted austenite fractions and compositions. Samples were annealed for 1 week with the sheets sealed in stainless steel bags containing titanium as an oxygen getter; water quenching was performed after heat treatment.

Room temperature tensile properties were measured using ASTM E-8[24] subsized tensile samples machined transverse to the rolling direction with a gage section of 25 mm. All tests were run at a constant engineering strain rate of 5.74×10^{-4} s^{-1}; duplicate samples were tested. Sample elongations were recorded with a 25-mm Shepic extensometer (John A. Shepic, Lakewood, CO).

Retained austenite contents were determined using a combination of X-ray diffraction (XRD) and neutron diffraction techniques. Samples for XRD were ground using standard metallographic techniques with silicon carbide grinding papers through 1200 grit followed by

Table I. Composition of Experimental Mn-TRIP Steel (Weight Percent)

C	Mn	Si	Cr	Ni	Mo	P	Al	N	S
0.099	7.09	0.13	0.04	0.03	0.01	0.015	0.031	0.008	0.008

polishing using a 3-μm diamond suspension. XRD measurements were performed using a copper X-ray source operating at 45 kV and 40 mA with a nickel filter; scans were run between 38 and 105 deg 2-theta to capture the significant ferrite and austenite diffraction peaks.

In-situ neutron diffraction measurements were made at the Lujan Center at Los Alamos National Laboratory in the SMARTS diffractometer[25] during tensile deformation on samples annealed at 848 K, 873 K, 898 K, and 923 K (575 °C, 600 °C, 625 °C, and 650 °C). Samples for the neutron diffraction experiments were surface ground with 600 grit silicon carbide paper to remove surface oxide. Measurements were recorded at fixed strain increments, where displacement was maintained constant and diffraction patterns were recorded with the sample under load; this procedure allowed bulk measurements of phase development with strain to be made on a single specimen for each annealing temperature. Samples were loaded in uniaxial tension transverse to the rolling direction. Retained austenite was determined by using Rietveld analysis[26,27] of the whole pattern to generate a fit that described the pattern for each phase; the integrated intensities were then determined for each phase and compared. For all diffraction experiments, martensite and ferrite were interpreted as the same body-centered-cubic phase since martensite doublets were not discernable in the data.

Metallographic analysis was performed using a 2 pct nital etch and scanning electron microscopy (SEM). All images are of the plane normal to the transverse direction with respect to the rolling direction.

III. RESULTS

A. *Microstructure*

Figure 2 shows the measured austenite fractions present at room temperature as a function of annealing temperature. Data for the 848 K to 923 K (575 °C to 650 °C) samples were obtained with neutron diffraction, while data for the 948 K (675 °C) condition were measured with XRD. The amount of retained austenite increased to 43.5 wt pct for the 923 K (650 °C) anneal and then decreased dramatically for the 948 K (675 °C) condition to around 1 wt pct. As shown in Figure 2, the experimentally measured effect of annealing temperature on austenite stability is similar in form to the predicted behavior and is consistent with the reported deviation reported by De Moor *et al.*[6] attributed to the kinetic effects on Mn enrichment. Table II includes a summary of the fraction of austenite as measured by diffraction and the ferrite fraction measured using point counting; the remaining structure was assumed to be martensite. The high fraction of austenite at the annealing temperature, and the correspondingly low Mn level in austenite, at 948 K (675 °C), likely resulted in low austenite stability on quenching producing a predominantly martensitic structure.

Figure 3 contains representative neutron diffraction patterns for the 848 K to 923 K (575 °C to 650 °C) conditions both in the quenched condition and after straining. Ferrite and austenite peaks are readily identified in the patterns and are indexed. Limited amounts of epsilon martensite were observed in the quenched structures for the 898 K and 923 K (625 °C and 650 °C) samples; no epsilon peaks were observed for the 848 K or 873 K (575 °C or 600 °C) condition (Figure 4). Similarly, XRD measurements did not reveal the presence of epsilon for the 949 K (675 °C) condition; only ferrite peaks were observed with the exception of the austenite 220 reflection. Epsilon was observed in the 873 K (600 °C) condition using XRD; however, this may have been a result of sample preparation and an artifact of the surface measurement compared to the bulk measurements made using neutron diffraction. In the neutron diffraction data, limited amounts of epsilon martensite not present in the unstrained condition appeared with strain, as can be seen by the evolution of the ε_{002} peak in Figures 3(c) and (d).

Table II. Phase Fractions Measured in Each Condition

Annealing Temperature (K)	Annealing Temperature (°C)	Austenite (Wt Pct)	Ferrite (Wt Pct)	Martensite (Wt Pct)
848	575	26.0	76	0
873	600	33.0	49	18
898	625	40.0	54	6
923	650	43.5	34	22.5
648	675	1.4	20	78.6

Figure 5 contains secondary electron micrographs of the heat-treated microstructures. The microstructural constituents in the quenched structures are primarily ferrite (F), martensite (M), and retained austenite (A), the amounts of each varying systematically with heat treatment. The annealing response of the initial cold-rolled martensitic microstructure produced relatively fine-grained annealed, even after the 1 week annealing treatment. At the lower temperatures, this was likely a product of the fine recrystallized grain size and the two-phase nature present during heat treatment, constraining grain boundary movement.

Figure 5(a) shows the microstructure after annealing at 848 K (575 °C). The microstructure consisted of 76 vol pct ferrite with an approximate ferrite grain size of 0.9 μm. Austenite was present as separated islands, identified as smooth features, and interlath with martensite in the finely etched regions (labeled M/A in the figure). Figures 5(b) and (c) show the 873 K and 898 K (600 °C and 625 °C) microstructures, respectively; a fine ferrite grain structure is apparent, 49 and 54 vol pct respectively, with distributed pools of mixed martensite and austenite. While the austenite is not distinctly separate in the structure, it is interpreted that it is subdivided within the martensitic lath structure.

Annealing at 923 K (650 °C) (Figure 5(d)) resulted in a microstructure composed primarily of mixed martensite-austenite with individual austenite blocks apparent in the etched regions. The sample responded differently to the etching solution than samples heat treated at lower temperatures. This sample possessed the highest volume

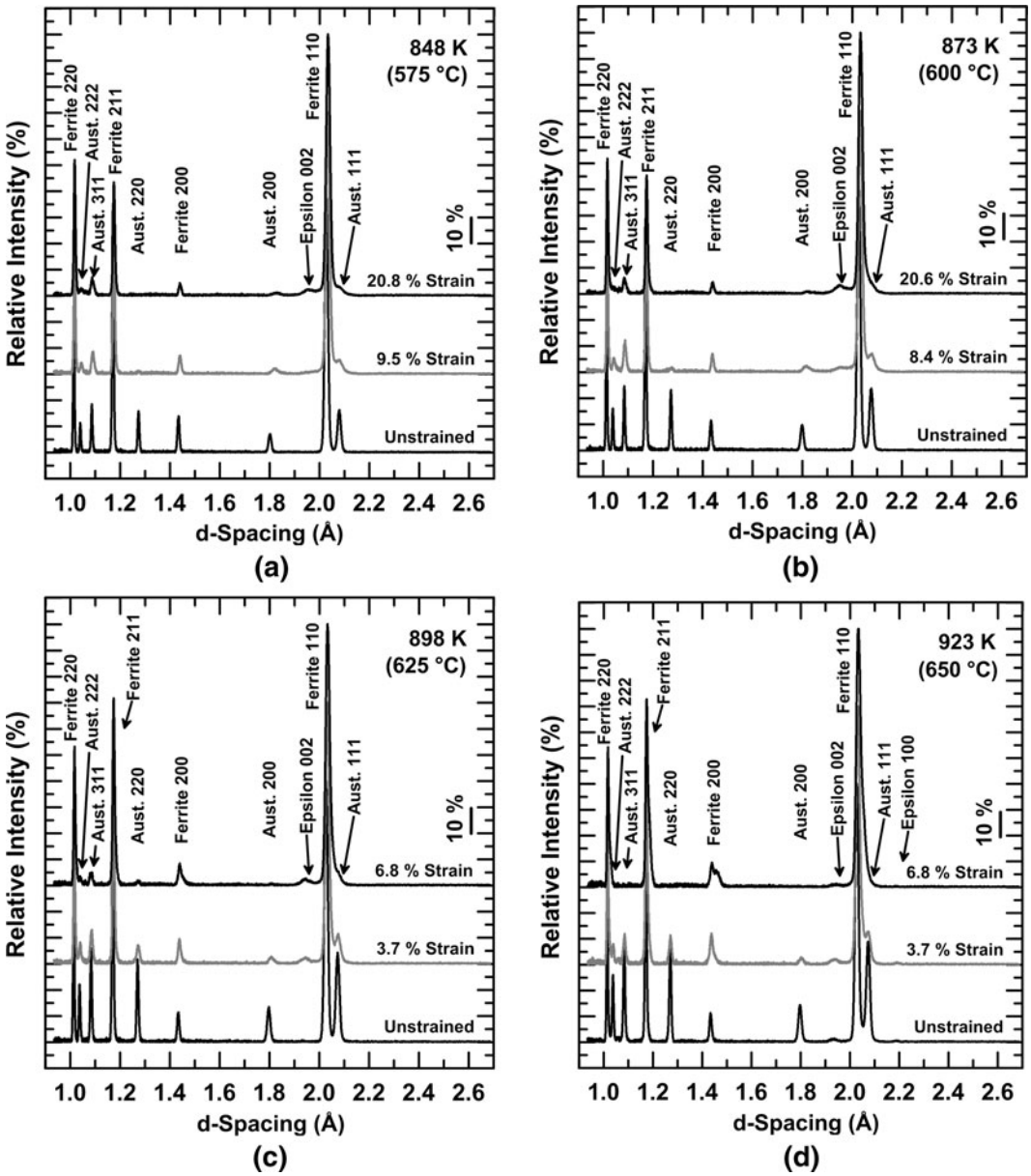

Fig. 3—Representative neutron diffraction patterns during straining for (*a*) 848 K (575 °C), (*b*) 873 K (600 °C), (*c*) 925 K (652 °C), and (*d*) 923 K (650 °C).

fraction austenite (Figure 2); the high austenite fraction may be responsible for the change in etching response. The 948 K (675 °C) heat treatment resulted in an apparent dual-phase ferrite-martensite structure (Figure 5(e)), with minimal amounts of retained austenite as measured in the XRD data (Figure 2). The dual phase constraint on grain boundary movement was insufficient to constrain grain growth at the highest temperature, and a ferrite grain size of approximately 1.5 μm was produced.

B. *Tensile Properties*

Figure 6(a) shows representative engineering stress-strain behavior for all annealing temperatures. Table III summarizes tensile data (0.2 pct offset or upper yield stress, ultimate tensile strength (UTS), yield to tensile ratios, and total elongation) obtained from duplicate tensile tests and shows that excellent reproducibility was observed for all test conditions. The tensile data illustrate significant systematic changes in deformation behavior with annealing temperature, which are amplified in Figure 6(b), which expands the low strain region to highlight differences in yielding behavior between the five conditions. Observed differences in the strain hardening behavior during continuous deformation (*i.e.*, beyond the yield point elongation (YPE) region for those samples that exhibited YPE) are shown in Figure 7, which presents Jaoult–Crussard analyses[28,29] of the true working hardening rate of the annealed structures as a function of strain. In Figure 7, the

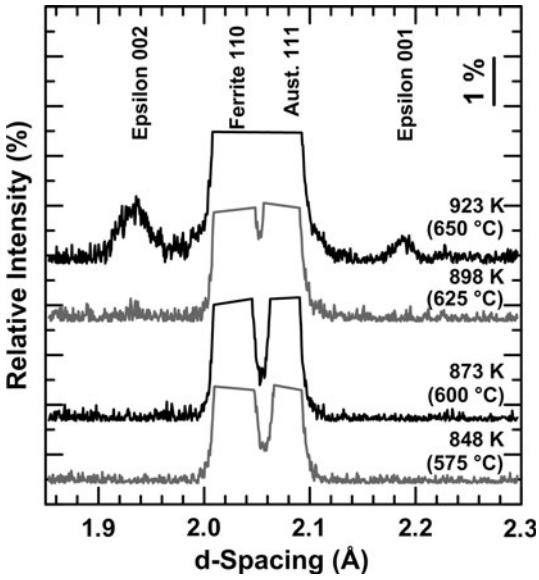

Fig. 4—Neutron diffraction patterns highlighting the presence of epsilon martensite in the quenched structures after intercritical annealing at the temperatures listed in the figure.

logarithm of the true work hardening rate is plotted *vs* the logarithm of the true plastic strain, and work hardening behavior differences, particularly at low strains, are amplified to illustrate regimes in strain hardening.[26] Figures 6 and 7 show that the tensile stress-strain response of the heat-treated microstructures varies significantly with annealing temperature consistent with the results obtained by Merwin and others.[11–18]

The sample annealed at 848 K (575 °C) exhibited the highest yield stress (around 770 MPa), significant YPE followed by limited strain hardening, and a total elongation of approximately 35 pct. The behavior of this condition is similar to the observed stress-strain response of ultra-fine-grained duplex[9] and ferritic[31] steels. The low work hardening rate suggests limited contribution of deformation-induced transformation of austenite to martensite.

With an increase in annealing temperature, the yield strength (YS) and extent of discontinuous yielding decrease while the strain hardening rate during continuous deformation and UTS increase. The 873 K (600 °C) condition exhibited a well-defined yield point

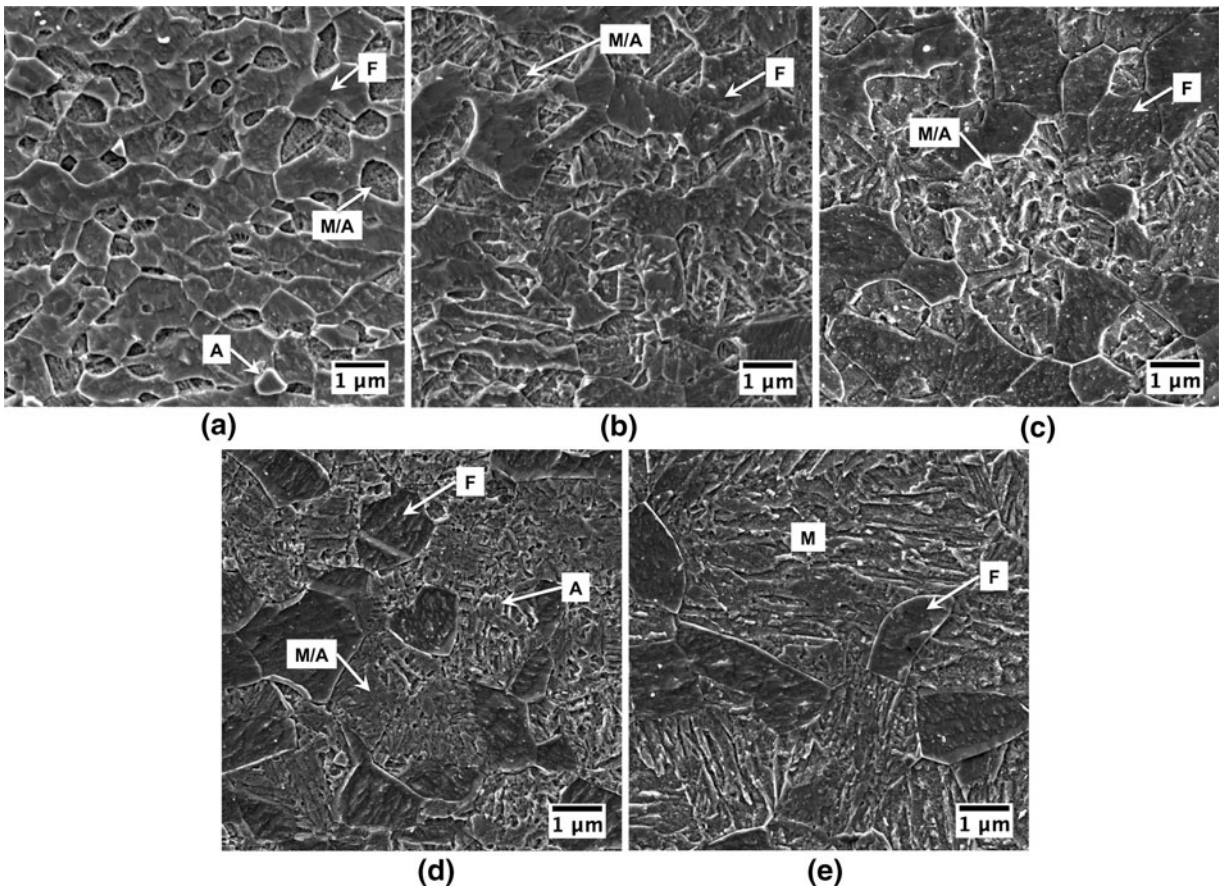

Fig. 5—Secondary electron SEM micrographs for the 7.1-Mn steel annealed at (*a*) 848 K (575 °C), (*b*) 873 K (600 °C), (*c*) 898 K (625 °C), (*d*) 923 K (650 °C), and (*e*) 948 K (675 °C) for 1 week and quenched. 2 pct Nital etch. Representative phase regions are labeled ferrite (F), martensite (M), austenite (A), and mixed martensite and austenite (M/A).

followed by discontinuous yielding characteristics of annealed ferrite deformation. Immediately following discontinuous yielding, the work hardening rate initially increased with strain, as shown in Figure 7(a). This was followed by strain-dependent work hardening that decreased and then increased with increasing strain; serrations appeared in the stress-strain behavior leading to fluctuations in work hardening for strains above 0.1. This sample exhibited the highest ductility observed in all of the tensile samples with a UTS of approximately 900 MPa and a total elongation over 40 pct.

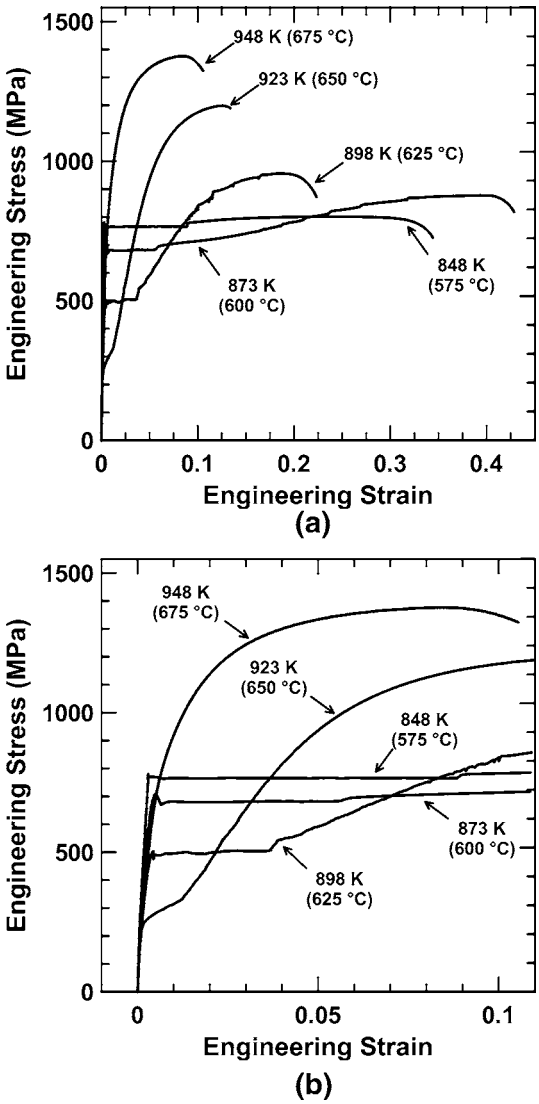

Fig. 6—(*a*) Tensile engineering stress-strain curves and (*b*) magnified yielding behavior for 7.1-Mn steel annealed for 1 week at the temperatures indicated in the figures. Samples tested at a constant engineering strain rate of 5.74×10^{-4} s^{-1} using ASTM E-8 subsized samples with a 25-mm gage length.[23]

Increasing annealing temperature further to between 898 K and 948 K (625 °C and 675 °C) resulted in the extent of YPE decreasing with increasing annealing temperature, disappearing completely above 923 K (650 °C). This progressive change in yielding behavior is similar to that observed in DP steels. The apparent inflection in work hardening observed at a strain of approximately 0.02 in the 923 K (650 °C) sample was observed previously and was shown to be associated with the propagation of a very diffuse Lüders band[32] in studies of dual-phase steels and austenite transformation in Mn-TRIP steels.[33] The yield stress decreased with annealing temperature up to 923 K (650 °C), where the lowest yield stress of 270 MPa was observed. The sample annealed at 948 K (675 °C) exhibited continuous yielding, a high 0.2 pct offset yield stress of 759 MPa, a high initial work hardening rate leading to the lowest total elongation, and limited postuniform elongation.

Figure 8 correlates the dependence of tensile properties on processing temperature with measured austenite contents, where Figure 8(a) compares YS and UTS with austenite content and Figure 8(b) considers changes in the strength-ductility product. The strength-ductility product (UTS × total elongation), a measure of "toughness" during plastic deformation, is often used[33] to identify optimal sheet steel property combinations. Data for the 948 K (675 °C) material are not included here due to the low (<2 pct) austenite content. Figure 8(a) highlights the importance of retained austenite on the resulting properties as the yield and tensile strengths diverge with an increase in austenite content. The peak in the data shown in Figure 8(b) is for the material annealed at 873 K (600 °C), *i.e.*, the condition with the maximum ductility shown in Figure 6(a).

C. *Austenite Stability*

Figure 9 presents the fraction of austenite as a function of strain for 848 K to 923 K (575 °C to

Table III. Summary of Recorded Tensile Properties for Annealed 7.1-Mn TRIP Steels

Annealing Temperature (K)	Annealing Temperature (°C)	YS 0.2 Pct Offset or Upper YP (MPa)	UTS (MPa)	YS/UTS (Pct)	Total Elongation in 25 mm Gage (Pct)
848	575	769	800	96	34
848	575	763	800	95	32
873	600	679	871	78	41
873	600	710	876	81	42
898	625	503	954	53	22
923	650	276	1219	23	10
923	650	268	1197	22	10
923	650	266	1198	22	12
948	675	759	1360	56	5
948	675	790	1376	57	9

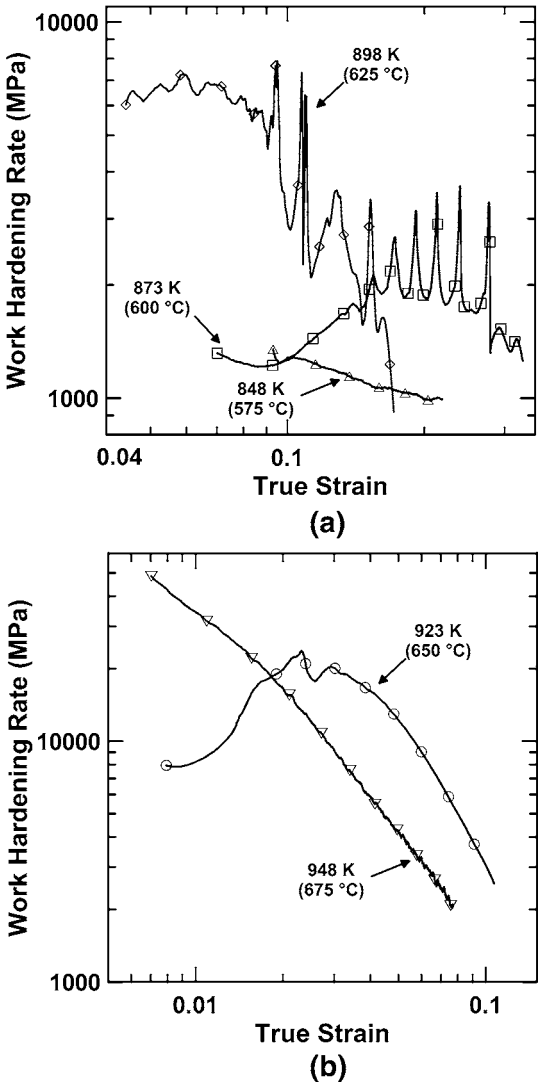

Fig. 7—Jaoult–Crussard analysis of instantaneous true work hardening rate *vs* true strain for (*a*) 848 K to 898 K (575 °C to 625 °C) and (*b*) 923 K and 948 K (650 °C and 675 °C) heat treatments.[24–26] Data are plotted on a log-log scale.

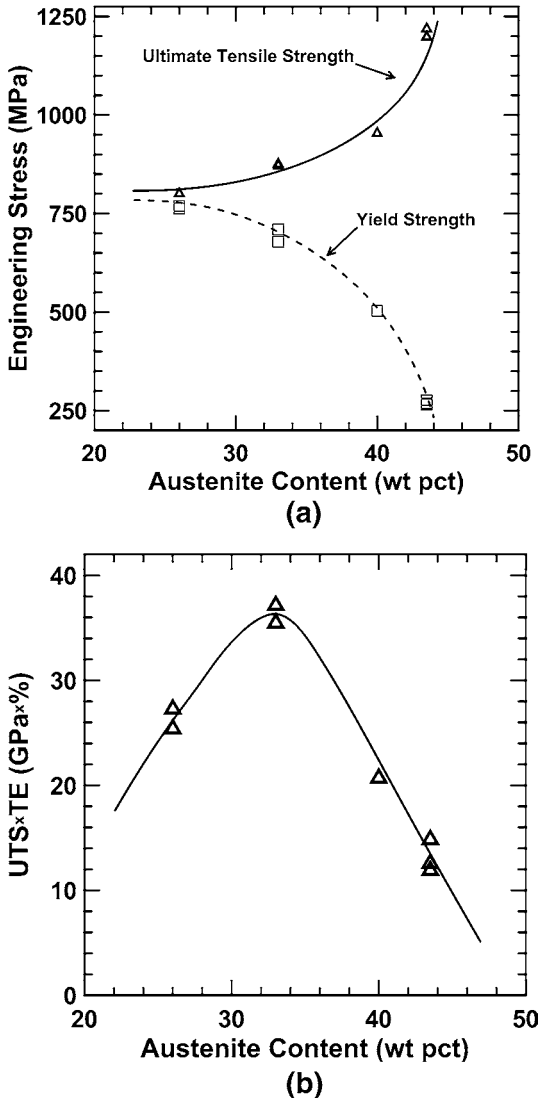

Fig. 8—Comparison of (*a*) YS and UTS and (*b*) strength ductility product *vs* austenite fraction after annealing 1 week at temperatures between 848 K and 923 K (575 °C and 650 °C).

650 °C) conditions as measured with *in-situ* neutron diffraction; Figure 9(b) presents the observed behavior at low strains. The data show that the mechanical stability of austenite in the annealed sheets depends significantly on annealing temperature. The austenite produced after annealing at 848 K (575 °C) was very stable with strain, resulting in approximately 3/4 of the initially retained austenite remaining after 20 pct strain. In contrast, the 873 K to 923 K (600 °C to 650 °C) conditions display progressively decreasing austenite stability with increasing annealing temperature. Low mechanical austenite stability was observed for the 898 K and 923 K (625 °C and 650 °C) annealing temperatures, as large fractions of the initially retained austenite transformed at low strains (*i.e.*, <8 pct strain) during uniform deformation. The austenite in the 873 K (600 °C) annealed material exhibited behavior distinctly different from that observed at higher or lower temperatures. Over the strain range investigated, approximately 2/3 of the austenite transformed, but much of this transformation occurred at strains well above 10 pct. Neutron diffraction measurements below the YS showed no change in austenite fraction with increasing stress. Austenite transformation only occurred after the onset of plastic flow, suggesting that the contribution of stress-assisted transformation was minimal.

D. *Austenite Transformation Kinetics*

Numerous models have been suggested to represent austenite transformation with strain in metastable TRIP steels. Two models, the Burke–Matsumura (BM) and Olson–Cohen (OC) models, for strain-induced austenite transformation were used here.[19–21] Both models were successfully applied[19–23] to a range of steels with metastable austenite and varying mechanical stability, including multiphase TRIP steels.

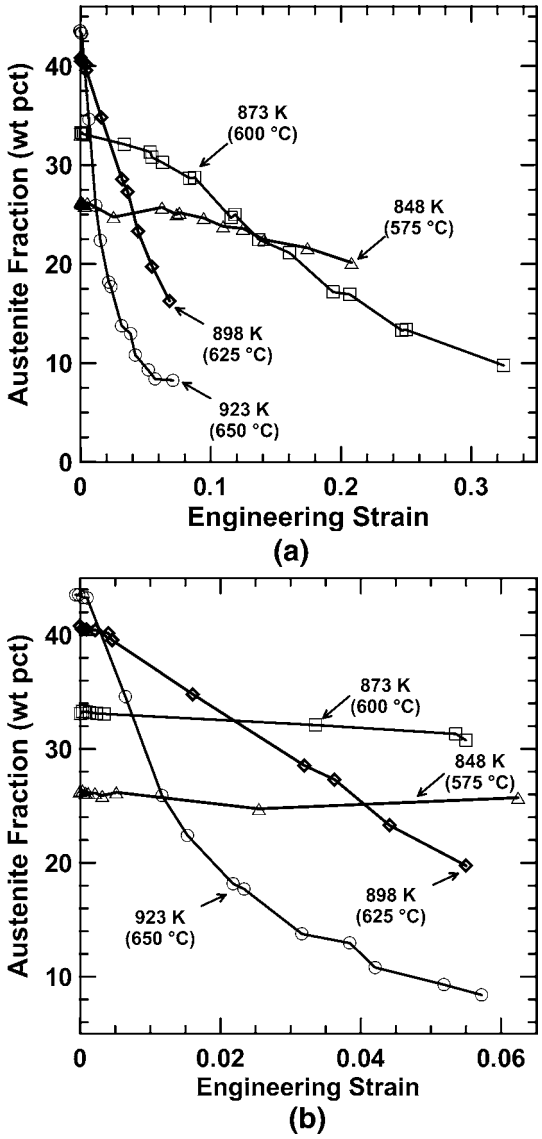

Fig. 9—Plot of austenite fraction as a function of strain for the 7.1-Mn steels intercritically annealed at the temperatures listed for (*a*) a full range of measured strain and (*b*) low strain levels.

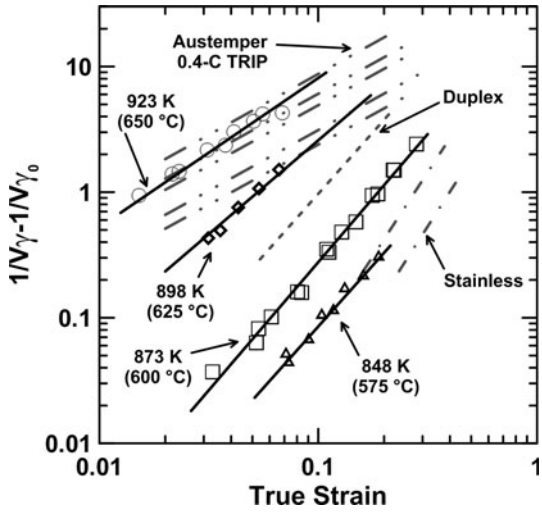

Fig. 10—Austenite transformation kinetics for Mn-TRIP steel annealed 1 week at the temperatures listed as fit using the BM model and compared to values from the literature.[20,21,34,35] Fit curves extrapolated to the recorded uniform elongation of each condition.

The BM model is a modification of diffusional transformation kinetics models for austenite decomposition where strain replaces transformation time. If strain is assumed to increase monotonically, then austenite fraction can be represented by Eq. [1], where the parameters p and k are empirically related to transformation kinetics and thermodynamic driving force, respectively.[20,21]

$$\frac{1}{V_\gamma} - \frac{1}{V_{\gamma 0}} = \frac{k}{p} * \varepsilon^p \qquad [1]$$

The value of p is related to the likelihood of austenite transformation with strain; low values of p indicate that the transformation is rapid with strain, while increasing p values decrease the effect of strain on the transformation rate. The value of p is also related to various microstructural features (such as quenched martensite, bainite, or ferrite), which may alter strain-induced martensite nucleation.[21] The parameter k is related to the relative stability of austenite with strain; higher values of k correlate to higher driving forces for transformation and lower austenite stabilities. Both of these constants are taken to be independent of strain.

The results for fitting the BM model to the experimental data are presented in Figure 10; for this figure, the log of Eq. [2] was taken so that the slope of the line is p and the y-intercept is $\log(k/p)$. Also plotted in Figure 10 are data from the literature for an austempered 0.4 wt pct C TRIP with 12 to 19 pct austenite,[21] a duplex stainless steel with 50 pct austenite,[34] and a fully austenitic metastable stainless steel.[35] Additionally, Table IV summarizes the fit parameters with several comparisons to the literature. The fit values for the current work fall within the range of those reported for these various steels. For the investigated heat treatments, k increases with annealing temperature, indicating lower austenite stability, while p decreases suggesting an increase in martensite nucleation rate.

The OC model for strain-induced austenite transformation assumes that shear band intersections act as martensite nuclei.[19] The strain-induced fraction transformed is calculated according to Eq. [2]:

$$f_{\alpha'} = 1 - \exp[-\beta(1 - \exp[-\alpha\varepsilon])^n] \qquad [2]$$

where α is related to the rate of shear band formation, and thereby the stacking fault energy of the austenite and the test strain rate, while β is related to the probability of martensite nucleation at a shear band intersection, which is dependent on the chemical driving force for austenite to martensite transformation and the necessary strain energy of the transformation.[19] The parameter n is a geometric constant relating the orientation of shear bands and the probability of shear band intersection. Low values of β indicate either a low probability of transformation on a nucleation site due to

Table IV. BM Model Parameters for Various TRIP Steels

Condition		Fraction Austenite (wt pct)	k	p	Ref
Current work	848 K (575 °C)	26.3	14.9	1.95	—
	873 K (600 °C)	33.3	61.7	2.04	—
	898 K (625 °C)	40.3	120	1.49	—
	923 K (650 °C)	43.5	148	1.19	—
Stainless Steel	LA	100	51	3	35
	LF	100	183	3	35
Austempered TRIP	TRIP 1	17.5	65	1	21
	TRIP 2	19.2	52	1	21
	TRIP 3	17.1	33	1	21
	TRIP 4	16.9	25	1	21
	TRIP 5	12	94	1	21
Quenched and partitioned	Q&P 1	7.7	16	0.52	23
	Q&P 2	11.2	33	0.71	23
	Q&P 3	14.8	120	1.17	23

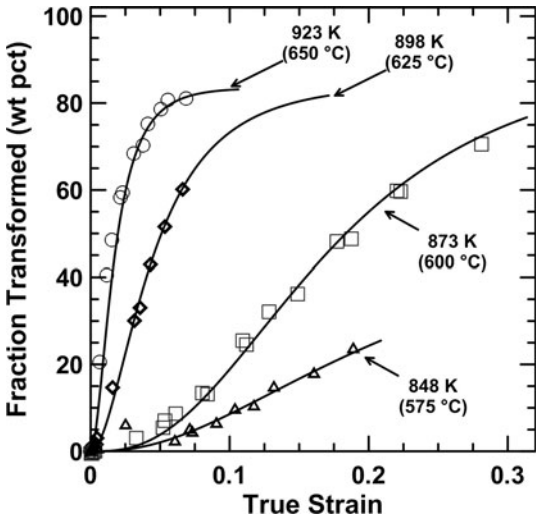

Fig. 11—Evolution of austenite transformation with curve fits based on the OC model. Measurements made using neutron diffraction. Fit curves extrapolated to the recorded uniform elongation of each condition.[19]

orientation or geometry effects or a low driving force for transformation. Both α and β are temperature dependent. The value of n acts to modify the number of shear bands in a given volume that can form nucleation sites.[19] An n value of 2 represents a random distribution of shear band orientations, while n values greater than 2 correspond to some degree of parallelism of the shear bands, slowing the transformation rate.

Figure 11 shows austenite fraction decomposed as a function of true strain along with curve fits based on the OC model; the corresponding α, β, and n values are listed in Table V. Additionally, Table V includes comparisons between this work and values found in literature.[19,22,23,36] The fit parameters for the steels considered here are consistent with those obtained with the BM model, with decreased austenite stability (higher β) and a pronounced change in transformation behavior with increasing α and decreasing n occurring with an increase in annealing temperature.

IV. DISCUSSION

The effects of the long-time heat treatments on Mn enrichment of austenite are evident in the resulting microstructural constituents; significant fractions of austenite (26 to 43 wt pct) were successfully stabilized. In the quenched structures, there was little evidence of martensite (either ε or α') in the diffraction data for 848 K and 873 K (575 °C and 600 °C) conditions, while ε martensite was observed in the 898 K and 923 K (625 °C and 650 °C) conditions. Since α' was not distinguishable from ferrite in the diffraction data, it may have been present in the 898 K and 923 K (625 °C and 650 °C) annealed conditions. Only ferrite, α' martensite, and a residual amount of austenite were observed in the 948 K (675 °C) condition. Merwin[13] also observed ε martensite using electron backscatter diffraction techniques in the SEM. The amount of ε on cooling increased with increasing annealing temperature to approximately 1.6 wt pct for samples annealed at 923 K (650 °C); the amount of observed ε then decreased rapidly with increasing annealing temperatures.

The progression of phases with heat treatment temperature may be explained when considering published binary Fe-Mn phase maps[37,38] describing deformed microstructure constituents. These maps predict that Mn contents lower than 10 pct result only in α' martensite, while between 10 and 15 pct Mn, both α' and ε martensite develop. In higher Mn steels, *i.e.*, above 15 wt pct, austenite-ε mixtures are expected. The predicted equilibrium Mn contents in austenite for the current work, shown in Figure 1, are 15 pct for the 848 K (575 °C) anneal; 13 and 11 for the 873 K and 898 K (600 °C and 625 °C) anneal, respectively; and 9.5 and 8 pct for the 923 K and 948 K (650 °C and 675 °C) annealing temperatures.

While the steel used in this work included elements in addition to Fe and Mn, the published binary Fe-Mn phase maps provide some insight into the effectiveness of the Mn-enrichment treatments. The reasonable agreement between the observed phases in the neutron diffraction data (Figure 3) and the expected phases from

Table V. OC Model Parameters for Various TRIP Steels

Condition		Fraction Austenite (Wt Pct)	n	α	β	Ref.
Current work	848 K (575 °C)	26.3	2.67	6.37	0.67	
	873 K (600 °C)	33.3	3	5.75	2.5	
	898 K (625 °C)	40.3	2	18.6	1.86	
	923 K (650 °C)	43.5	2	49.5	1.8	
Stainless steel	304 SS 20 °C	100	4.5	3.53	0.52	19,36
Banitic TRIP	CMnSi-TRIP	16	2	31.2	1.82	22
	CMnAl-TRIP	14	2	12.7	1.49	22
	CMnSiAl-TRIP	18	2	20.9	1.49	22
	CMnSiAlP-TRIP	13	2	8.6	1.6	22
Quenched and partitioned	Q&P 1	7	2	71	0.46	23
	Q&P 2	11	2	52	0.63	23
	Q&P 3	15	2	21	4.02	23

the Fe-Mn maps indicate that a broad range of Mn contents were successfully produced with the various annealing temperatures. Diffusion rates of Mn in steel are generally low and the resulting kinetics of Mn enrichment to austenite would be expected to be slow. However, starting with a martensitic microstructure prior to annealing resulted in a fine-annealed structure: 0.9 to 1.1 μm ferrite in the range of microstructures here. As a consequence of the fine microstructure, the expected Mn diffusion distances for the applied heat treatments were likely sufficient to significantly enrich Mn in austenite,[5] a conclusion consistent with the recent work by Lee *et al.*[39]

The range of austenite compositions in austenite produced by the enrichment treatment likely resulted in the change in austenite stability and strain-hardening behavior with annealing temperature. Figures 5 through 8 highlight the dependence of stress-strain behavior and strain hardening on annealing temperature. Similar variations in behavior were also observed in previous studies.[11–16,18] High YS and low work hardening are observed at low annealing temperatures evolving to low YS and high work hardening rates with increasing annealing temperature. The effect of decreasing Mn content in austenite with increasing annealing temperature and the related effect of Mn on austenite stability may explain this progression in behavior.

The higher Mn (15 to 30 wt pct) steels examined by Frommeyer *et al.*[40] and Grässel *et al.*[41] also highlight the effect of Mn content on austenite deformation behavior for fully austenitic mixed TRIP/TWIP steels. Lower Mn content was correlated to an increased strain-induced transformation rate, which increased strain hardening rates. This trend is similar to that seen in the progression of behaviors displayed by annealing between 848 K and 923 K (575 °C and 650 °C) in the present work, where strain hardening rates increased with decreasing predicted Mn content in austenite.

The importance of the combined effects of austenite stability and volume fraction in the deformation behavior of Mn-modified TRIP steels is clarified through Figure 12, which correlates strain hardening behavior with austenite stability for samples annealed at 848 K, 873 K, and 923 K (575 °C, 600 °C, and 650 °C). Figure 12 highlights that for samples in which

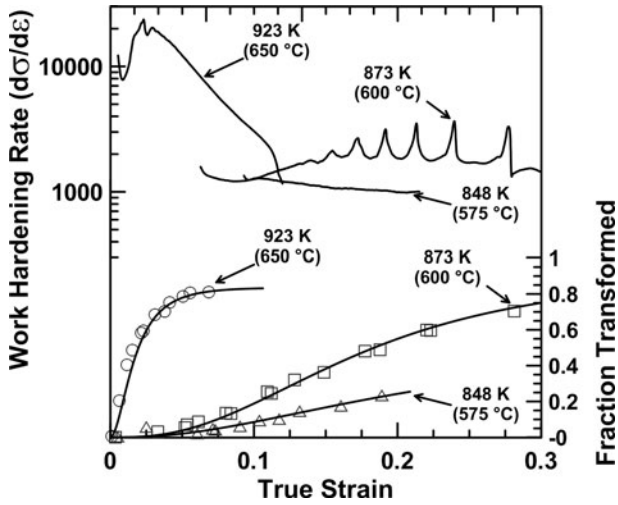

Fig. 12—Comparison between instantaneous true work hardening rate ($d\sigma/d\varepsilon$) and austenite decomposition kinetics. Curve fits for the austenite fraction transformed are based on the OC model.[19]

strain-induced martensite forms (as opposed to stress-assisted martensite formation[42,43]), variations in work hardening may be correlated to changes in the austenite transformation behavior. Periods of rapid austenite transformation relate to rapid work hardening, while sluggish austenite transformation has little effect on work hardening.

The high transformation rate exhibited by the 923 K (650 °C) samples leads to the highest observed work hardening rates and deformation behavior that mirrors high martensite volume fraction DP steels.[30] The values α, β, and k from the modeled transformation curves were generally high for this condition, indicating a high driving force with minimal kinetic barrier for austenite transformation to martensite.

The 848 K (575 °C) condition steel contained austenite with the maximum stability, which resulted in limited contributions of the TRIP effect (*i.e.*, strengthening due to martensite formation with strain) and an almost "flat" stress-strain curve. The flat stress-strain curve is markedly similar to the behavior of ultra-fine-grained steels,[31,44–47] where low work hardening rates were attributed to the inability of dislocation cell formation in

the fine grains. While the microstructure shown in Figure 5(a) differs from a "true" ultra-fine-grained steel (*i.e.*, grain size <1 μm[44,46]), it is likely that the scale is fine enough to retard dislocation cell formation contributing to the observed behavior. The model analysis for austenite transformation produced low β (OC model) and k (BM model) fit parameters, suggesting a low driving force for austenite decomposition with strain. This observation is as anticipated given the high Mn level predicted for annealing at 848 K (575 °C).

Figure 12 highlights the work hardening behavior in the sample annealed at 873 K (600 °C) compared to higher and lower temperature annealing treatments. At low strains, the work hardening rate is low and is similar to that observed for the 848 K (575 °C) sample, where limited austenite transformation occurred. However, with strain above 0.1, significant austenite transformation to martensite occurred, leading to work hardening rates significantly greater than those for the 848 K (575 °C) sample. For this annealing temperature, some initial strain is necessary to develop sufficient martensite nucleation sites; once these sites are present the austenite to martensite transformation occurs readily, contributing to the increased strain hardening. This behavior is reflected in the low α value (5.75) in the OC model fit, suggesting that the generation of nucleation sites may be sluggish and the high β value (2.5) indicated high driving force for transformation once sufficient nucleation sites are present. As a consequence of the higher work hardening rate at high strain, deformation was stabilized, leading to the highest observed total elongation of 40 pct.

A distinct change in behavior from the 873 K to 898 K (600 °C to 625 °C) conditions is observed where higher strain hardening at lower strain levels was observed for the higher temperature treatment, which exhibited limited austenite stability (Figure 11) similar to that observed in the 923 K (650 °C) sample. As a consequence of the higher initial work hardening rates and consistent with previous analyses,[30] the ductility in the 898 K (625 °C) sample is lower than for the 873 K (600 °C) sample (22 *vs* 42 pct). The austenite stability parameters from Tables IV and V for the sample annealed at 898 K (625 °C) are similar to those reported for TRIP steels, where austenite is stabilized by carbon partitioning during low-temperature processing.[21,22] The α value (18.6) from Table V for the 898 K (625 °C) sample is higher than for the 873 K (600 °C) condition (5.75), suggesting that martensite nucleation site generation is more rapid with strain.[19] Additionally, as characterized by the higher k parameter (120) from Table IV, the driving force for transformation in the 898 K (625 °C) sample is higher than in the steels annealed at lower temperatures and more characteristic of the sample annealed at 923 K (650 °C) with a k value of 148.

As highlighted in Figures 9 and 11, in samples where the available austenite is rapidly exhausted with strain, high initial strain hardening occurs, which leads to significant increases in strength and corresponding decreases in ductility. As a consequence, samples with the highest amount of initial austenite present at room temperature, the samples annealed at 898 K and 923 K (625 °C and 650 °C), exhibited the lowest UTS × TE products of approximately 21 and 13 GPa × pct, respectively.

For all the steels considered in this study, α in the OC model increased with annealing temperature (Table V). The dependence of α on annealing temperature may also relate to the effect of Mn content on the stacking fault energy (SFE), as α is directly dependent on the rate of shear band formation and thereby the SFE. However, the relationship between SFE and Mn is not clear.[48] In the binary Fe-Mn system, SFE was reported to exhibit a minimum value at approximately 15[49] or 12 wt pct.[50]

The material annealed at 923 K (650 °C) exhibited an unusually low yield point and unusually high α (OC model) and k (BM model) values. These combined behaviors could suggest that stress-assisted austenite transformation contributed to the initial yielding behavior. Additionally, the austenite transformation rate at very low strains was almost linear with strain (Figure 9(b)). This may also indicate the presence of a stress-assisted mechanism.[42,43] However, the neutron diffraction data at low stresses, near yielding, did not show a significant change in the austenite fraction until plastic deformation mechanisms were active, indicating that strain-induced austenite transformation is predominant. A more detailed study into the yielding behavior of this condition is necessary to separate the individual mechanisms.

V. CONCLUSIONS

Prolonged intercritical annealing of a 0.1C-7.1Mn steel produced a range of austenite fractions and tensile behaviors, ranging from high ductility with limited work hardening for the lowest test temperature, to high strain hardening behavior at the intermediate temperature, to very low ductility high strength materials at the highest annealing temperatures. This breadth of tensile properties is likely a result of varying austenite stability against strain-induced transformation generated by the varying C and Mn levels in austenite produced during the annealing treatment. Annealing at lower temperatures produced highly stable austenite and low strain hardening rates. Increasing annealing temperature resulted in progressively decreasing austenite stability and increased strain hardening due to the TRIP affect. Annealing at the higher test temperatures resulted in conditions where austenite stability was insufficient to postpone necking at high strains. These conditions produced high UTS levels, but the total ductility was generally low. The correlation between austenite stability and mechanical behavior highlights that the development of new steels to meet third generation AHSS demands must take into consideration austenite stability as well as austenite amount.[3,4]

ACKNOWLEDGMENTS

The authors gratefully acknowledge the support of the National Science Foundation under Award No.

CMMI-0729114 and the sponsors of the Advanced Steel Processing and Products Research Center, an industry/university cooperative research center at the Colorado School of Mines. This work also benefited from use of the Lujan Neutron Scattering Center at LANSCE, which is funded by the Office of Basic Energy Sciences (DOE). Los Alamos National Laboratory is operated by Los Alamos National Security LLC under DOE Contract No. DE AC5206NA25396. Additionally, the authors acknowledge U.S. Steel for providing the experimental material, D.W. Brown and T.A. Sisneros for their assistance with the neutron experiments, and the 2009 Neutron Scattering School at the Lujan Center for providing the opportunity for one author (Gibbs) to learn about the capabilities of neutron diffraction.

REFERENCES

1. "Advanced High Strength Steel Application Guidelines," International Iron and Steel Institute, Committee on Automotive Applications, Middletown, OH, www.worldautosteel.org.
2. E. De Moor, P.J. Gibbs, J.G. Speer, J.G. Schroth, and D.K. Matlock: *Iron Steel Technol*., 2010, Nov., pp. 1–11.
3. D.K. Matlock and J.G. Speer: *Proc. 3rd Int. Conf. on New Developments in Advanced High-Strength Steels*. H.C. Lee, ed., Korean Institute of Metals and Materials, Seoul, 2006, pp. 774–81.
4. D.K. Matlock and J.G. Speer: *Proc. Microstructure and Texture in Steels and Other Materials*, A. Haldar, S. Suwas, and B. Bhattacharjee, eds., Springer, London, 2009, pp. 185–205.
5. D.K. Matlock, P.J. Gibbs, J.G. Speer, R.H. Wagoner, and J.G. Schroth: *Proc. NSF CMMI Research and Innovation Conf*., NSF, Washington DC, 2009, paper for Grant No. 0729114.
6. E. De Moor, D.K. Matlock, J.G. Speer, and M.J. Merwin: *Scripta Metall*, 2010, vol. 64, pp. 185–88.
7. *THERMO-CALC Tcw5.0.2.30,* Computer Software, Thermo-Calc Software AB, PC, Stockholm, Sweden, 2009.
8. B. Lee and B. Sundman: *THERMO-CALC Steels Database V2*, Scientific Group Thermodata Europe, Stockholm, Sweden, 1999.
9. R.L. Miller: *Metall. Trans*., 1972, vol. 3, pp. 905–12.
10. H. Huang, O. Matsumura, and T. Furukawa: *Mater. Sci. Technol*., 1994, vol. 10 (7), pp. 621–26.
11. M.J. Merwin: SAE Technical Paper No. 2007-01-0336, SAE, Warrendale, PA, 2007.
12. M.J. Merwin: *Mater. Sci. Forum*, 2007, vols. 539–543, pp. 4327–32.
13. M.J. Merwin: *Proc. MS&T 2007*, Detroit, MI, Sept. 16–20, 2007, pp. 515–36.
14. T. Furukawa, H. Huang, and O. Matsumura: *Mater. Sci. Technol*., 1994, vol. 10 (11), pp. 964–69.
15. D. Shu, S. Park, C. Lee, and S. Kim: *Metall. Mater. Trans. A*, 2008, vol. 40A, pp. 264–68.
16. S. Kim: *Mater. Sci. Forum*, 2010, vols. 638–642, pp. 3313–18.
17. S.W. Lee, K.Y. Lee, and B.C. De Cooman: *Mater. Sci. Forum*, 2010, vols. 654–656, pp. 286–89.
18. B.C. De Cooman, S Lee, and S.S. Kumar: *Proc. 2nd Int. Conf. on Super-High Strength Steels*, Associacione Italiana di Metalluricia, Verona, Italy, Oct. 17–20, 2010.
19. G.B. Olson and M. Cohen: *Metall. Trans. A*, 1975, vol. 6A, pp. 791–95.
20. J. Burke: *Kinetics of Phase Transformations in Metals*, 1st ed., Pergamon Press, Oxford, United Kingdom, 1965, pp. 51–52.
21. O. Matsumura, Y. Sakuma, and H. Takechi: *Scripta Metall*., 1987, vol. 21, pp. 1301–06.
22. L. Samek, E. De Moor, J. Penning, and B.C. De Cooman: *Metall. Mater. Trans. A*, 2006, vol. 37A, pp. 109–24.
23. E. De Moor, S. Lacroix, A.J. Clarke, J. Penning, and J.G. Speer: *Metall. Mater. Trans. A*, 2008, vol. 39A, pp. 2568–95.
24. *2008 Annual Book of ASTM Standards,* vol. 03.01, *Metals-Mechanical Testing; Elevated and Low Temperature Testing; Metallography*, "Standard Test Methods for Tension Testing of Metallic Materials," ASTM E-8/E 8M–08, ASTM, Philadelphia, PA, pp. 64–88.
25. M. Bourke, D.C. Dunand, and E. Ustundag: *Appl. Phys. A: Mater. Sci. Proc*., 2002, vol. 74, pp. S1707–S1709.
26. H.M. Rietveld: *J. Appl. Cryst*., 1969, vol. 2, pp. 65–71.
27. A.C. Larson and R.B. Von Dreele: "GSAS. General Structure Analysis System," Report No. LAUR 86-748, Los Alamos National Laboratory, Los Alamos, NM, 1986.
28. B. Jaoult: *J. Mech. Phys. Solids*, 1957, vol. 5, pp. 95–114.
29. C. Crussard: *Rev. Metall. (Paris)*, 1953, vol. 10, pp. 697–710.
30. D.K. Matlock, G. Krauss, and F. Zia Ebrahimi: in *Deformation, Processing, and Structure*, G. Krauss ed., ASM, Metals Park, OH, 1984, pp. 47 and 87.
31. W.B. Morrison and R.L. Miller: *Proc. Ultrafine-Grain Metals,* J.J. Burke, ed., Syracuse, NY, 1970, pp. 183–211.
32. D.K. Matlock, G. Krauss, L.F. Ramos, and G.S. Huppi: in *Structure and Properties of Dual Phase Steels*, R.A. Kot and J.W. Morris, eds., TMS-AIME, Warrendale, PA, 1979, pp. 62 and 90.
33. H. Han, C. Oh, G. Kim, and O. Kwon: *Mater. Sci. Eng. A*, 2009, vol. 499, pp. 462–68.
34. T. Nakamura and K. Wakasa: *Tetsu-to-Hagané*, 1975, vol. 61, p. 69.
35. D.C. Ludwigson and J.A. Burger: *J. Iron Steel Inst*., 1969, vol. 192, p. 63.
36. T. Angel: *J. Iron Steel Inst*., 1954, vol. 177, p. 165.
37. H. Schumann: *Arch. Eisenhüttenwes*, 1967, vol. 38 (8), pp. 647–56.
38. Q. Gu, J. Van Humbeeck, and L. Delaey: *J. de Phys. IV*, 1994, pp. C3-135–C3-144.
39. S.-J. Lee, S. Lee, and B.C. De Cooman: *Scripta Metall*, 2010, vol. 64, pp. 649–52.
40. G. Frommeyer, U. Brüx, and P. Neumann: *ISIJ Int*., 2003, vol. 43, pp. 438–46.
41. O. Grässel: *Int. J. Plasticity*, 2003, vol. 16, pp. 1391–1409.
42. G.B. Olson: in *Structure and Properties of Dual Phase Steels*, R.A. Kot and J.W. Morris, eds., TMS-AIME, Warrendale, PA, 1979, pp. 391–424.
43. G.B. Olson and M. Cohen: *Metall. Trans. A*, 1982, vol. 13A, pp. 1907–14.
44. D.H. Shin: *Met. Mater. Int*., 2001, vol. 7, pp. 573–77.
45. P. Hodgson, M.R. Hickson, and R.K. Gibbs: *Mater. Sci. Forum*, 1998, vols. 284–286, pp. 63–72.
46. R. Song, D. Ponge, D. Raabe, J.G. Speer, and D.K. Matlock: *Mater. Sci. Eng. A*, 2006, vol. 441, pp. 1–17.
47. N. Tsuji: *Scripta Mater*., 1999, vol. 40, pp. 795–800.
48. L. Brake, G. Mertens, J. Penning, B.C. De Cooman, M. Liebeherr, and N. Akdut: *Metall. Mater. Trans. A*, 2006, vol. 37A, pp. 307–17.
49. H. Schumann: *Kristall und Technik*, 1974, vol. 9, pp. 1141–50.
50. Y.K. Lee and C.S. Choi: *Metall. Mater. Trans. A*, 2000, vol. 31A, pp. 355–60.